Paper No. 137. (quote when citing this article)
Eleventh World Conference on Earthquake Engineering
ISBN: 0 08 042822 3

ENGINEERING SIMULATION OF GROUND MOTIONS FROM AN EXTENDED RUPTURE

T. HARADA[1], T. TANAKA[2] and T. OHSUMI[3]

[1]Associate Professor, Dept. of Civil Engineering, Miyazaki University, 1-1 Gakuen Kibanadai Nishi, Miyazaki 889-21, JAPAN
[2]Engineer, Chodai Company, Tokyo 104, JAPAN
[3]Engineer, System Engineering Department, Research and Development Center, Nippon Koei Co., Ltd., 2304 Takasaki, Kukizaki-machi, Inashiki-gun, Ibaraki 300-12, JAPAN

ABSTRACT

This paper describes digital simulation methods of strong earthquake ground motions using a seismological model. The methods described in this paper are based on the spectral representation of stochastic wave in conjunction with the seismological stochastic source model with ω^{-2} property and the representation theorem of elastodynamics. Numerical examples demonstrate an applicability of the proposed methods into prediction of strong earthquake ground motions in areas where strong-motion data are sparse.

KEYWORDS

Simulation of ground motions; Green's function, Stochastic Processes; Seismological model; Earthquake ground motions.

INTRODUCTION

Over the past four decades, primarily two approaches have been adopted in evaluation of the strong earthquake ground motions for aseismic design of the engineered structures. One is to use the recorded strong motions. In some cases the recorded motions are modified to better represent local soil conditions. The second is to generate strong ground motions by combining an appropriate seismological model with information about the seismicity and geology of the site. Whereas the first method is applicable in regions where strong-motion data are rich, it is not as easily applicable in areas where strong-motion data are sparse. In this paper, the ground motion of a small earthquake is produced by a stochastic point source model with ω^{-2} property, while the motion of a large earthquake is generated by an extended source with finite dimensions.

GROUND MOTION USING A STOCHASTIC POINT SOURCE MODEL

Based on the spectral representation of stochastic wave, the non-stationary stochastic acceleration motion $a(t)$ with the evolutionary power spectrum $S_{aa}(t,\omega)$ can be simulated in the following fashion (Shinozuka *et al.*, 1987):

$$a(t) = \sqrt{2}\sum_{j=1}^{N_\omega}\sqrt{2S_{aa}(t,\omega_j)\Delta\omega}\cos(\omega_j t + \phi_j);\ \ \omega_j = j\Delta\omega;\ \ \Delta\omega = \frac{\omega_u}{N_\omega};\ \ j = 1,2,\ldots,N_\omega \qquad (1)$$

An upper bound of the frequency ω_u in Eq.(1) represents an upper cut-off frequency beyond which $S_{aa}(t,\omega_j)$ may be assumed to be zero for either mathematical or physical reasons. In Eq.(1), ϕ_j are

independent random phase angles uniformly distributed over the range $(0, 2\pi)$. Note that the simulated motion is asymptotically Gaussian as N_ω becomes large due to the central limit theorem. The evolutionary power spectrum of the earthquake ground acceleration motion using a stochastic source model takes the following form:

$$S_{aa}(t,\omega) = \frac{1}{2\pi}|W(t,\omega)|^2|A(\omega)|^2; \quad |A(\omega)| = CA_S(\omega)A_D(\omega)A_A(\omega) \tag{2}$$

where $|W(t,\omega)|$ is the modulating function which defines the evolutionary power spectrum from the stationary power spectrum. $|A(\omega)|$ is the acceleration spectrum (Fourier amplitude spectrum) of the shear waves at a distance R from a fault with seismic moment M_0 which is given by Hanks and McGuire (1981). In Eq.(2), C, $A_S(\omega)$, $A_D(\omega)$, and $A_A(\omega)$, represent a scaling factor, a source spectrum, a diminution factor, and a local soil amplification factor, respectively. The scaling factor and the source spectrum are given by:

$$C = \frac{R(\theta,\varphi)FV}{4\pi\rho C_S^3}; \quad A_S(\omega) = \frac{M_0\omega^2}{1+(\omega/\omega_c)^2} \tag{3}$$

where $R(\theta,\varphi)$ is the average correction factor for radiation pattern, F accounts for free-surface amplification, V accounts for the partitioning of the energy in two horizontal components, ρ is the density of the material at the source, C_S is the shear wave velocity at the source, and ω_c is the corner frequency. The diminution factor and the local soil amplification factor are given by:

$$A_D(\omega) = \frac{1}{1+(\omega/\omega_{max})^n}\frac{1}{R}\exp(-\frac{\omega R}{2QC_S}); \quad A_A(\omega) = \frac{\sqrt{1+4h_g^2(\frac{\omega}{\omega_g})^2}}{\sqrt{(1-(\frac{\omega}{\omega_g})^2)^2+4h_g^2(\frac{\omega}{\omega_g})^2}} \tag{4}$$

The first factor in $A_D(\omega)$ is the high-cut filter that accounts for the sudden drop that the spectrum exhibits above ω_{max}. It is assumed here $n = 1$. The second factor is the geometric spreading factor of the shear wave. The third factor is the effect of the material damping on wave propagation in which Q is a frequency-dependent attenuation factor. In this paper the local soil amplification factor $A_A(\omega)$ is based on the Kanai-Tajimi spectrum (Kanai, 1957; and Tajimi,1960). ω_g and h_g control the peak position and the peak value of the amplification factor; $\omega_g = 15.6$(rad/sec), $h_g = 0.6$ for a firm soil. The modulating function $|W(t,\omega)|$ in Eq(2) is assumed here to be in the following form:

$$|W(t,\omega)| = \frac{e^{-(c_1\omega+c_2)t} - e^{-(c_3\omega+c_4)t}}{e^{-(c_1\omega+c_2)t^*} - e^{-(c_3\omega+c_4)t^*}}; \quad t^* = \frac{\ln(c_1\omega+c_2)-\ln(c_3\omega+c_4)}{(c_1\omega+c_2)-(c_3\omega+c_4)} \tag{5a}$$

where

$$c_k = [(a_{k1}\Delta - a_{k2})M + a_{k3} - a_{k4}\Delta] \times a_{k5}; \quad a_{11} = a_{31} = 6.0;\ a_{12} = a_{32} = 1600.0; \tag{5b}$$

$$a_{13} = 14000.0;\ a_{14} = a_{34} = 54.0;\ a_{15} = a_{35} = 10^{-6};\ a_{21} = a_{41} = 4.0;\ a_{22} = a_{42} = 1000.0; \tag{5c}$$

$$a_{23} = 9500.0;\ a_{24} = a_{44} = 36.0;\ a_{25} = a_{45} = 10^{-4};\ a_{33} = 15000.0;\ a_{43} = 9510.0 \tag{5d}$$

The form of the modulating function in Eq.(5) is determined in such a way that the equation approximates the evolutionary spectrum model developed by Kimura and Kameda (1987).

It should be noted here that in the low frequency range the acceleration spectrum $|A(\omega)|$ and the corresponding velocity and displacement spectra, $|V(\omega)|$ and $|U(\omega)|$, are proportional to ω^2,ω, and a constant, respectively. The Kanai-Tajimi spectrum of ground acceleration motion is constructed by multiplying $A_A(\omega)$ in Eq.(4) into a constant spectrum which represents the spectrum of acceleration motion at the base rock of the surface soil layer. Therefore, the singularities are present in the Kanai-Tajimi spectrum at $\omega = 0$, which cause the stationary variances of ground velocity and ground displacement to be unbounded. To remove these undesirable singularities, a filter is introduced by Clough and Penzien (1975). However, the physical meaning of the parameters in the filter of Clough and Penzien is still uncertain. The spectrum presented in Eq.(2) overcomes the undesirable singularities of the original Kanai-Tajimi spectrum without suffering from the physical meanings of the model parameters.

GROUND MOTION FROM AN EXTENDED FAULT

Simulation Method

This simulation method belongs to the empirical Green's function method initially suggested by Hartzell (1978). This method, which has been discussed in detail by Irikura (1983), is a method to simulate ground motions from an extended fault on the basis of the representation theorem of elastodynamics. In this paper, a brief discussion of the relevant mathematical formulation is presented in the frequency domain, and a new transfer function is presented, which accounts for the difference between the slip time function of the extended fault and that of the small fault. The extended fault surface with length L and width W is divided into small faults with length ΔL and width ΔW, as shown in Fig.1. Using the representation theorem of elastodynamics, the far-field displacement $\boldsymbol{u}(\boldsymbol{x},t)$ in a homogeneous, isotropic, and layered medium can be expressed in the following integral form (Aki and Richards, 1980; Somerville,*et al.*, 1991; Saikia, 1993):

$$\boldsymbol{u}(\boldsymbol{x},t) = \sum_{m=1}^{N_L}\sum_{n=1}^{N_W}\int_{\xi_m}^{\xi_m+\Delta L}\int_{\eta_n}^{\eta_n+\Delta W} \dot{D}(\xi_m,\eta_n,t-\tau_{mn}) * \boldsymbol{G}(\boldsymbol{x},\xi_m,\eta_n,t-t_{mn})d\xi d\eta \tag{6}$$

where $\boldsymbol{x} = (x,y,z)^T$ is the observation point, $\dot{D}(\xi,\eta,t)$ is the velocity of the source time function at position (ξ,η) on the fault, $\boldsymbol{G}(\boldsymbol{x},\xi,\eta,t-t_{\xi\eta})$ is the Green's function (the impulse response of the medium), and $*$ represents a convolution. τ_{mn} is the rupture propagation time from the hypocenter of the extended fault to the $(m,n)^{th}$ small fault, and t_{mn} is the propagation time for shear waves to travel from the $(m,n)^{th}$ small fault to the observation point, which are defined by:

$$\tau_{mn} = \frac{\zeta_{mn}}{V_R};\ \ t_{mn} = \frac{R_{mn}-R}{C_S} \tag{7}$$

where ζ_{mn} is the distance from the hypocenter of the extended fault to the $(m,n)^{th}$ small fault, R_{mn} is the distance from the $(m,n)^{th}$ fault to the observation point, R is the hypocentral distance of the extended fault, V_R is the rupture velocity of the fault, and C_S the S wave velocity of the medium.

The Fourier transform of Eq.(6) yields the following equation:

$$\boldsymbol{u}(\boldsymbol{x},\omega) = \sum_{m=1}^{N_L}\sum_{n=1}^{N_W}\int_{\xi_m}^{\xi_m+\Delta L}\int_{\eta_n}^{\eta_n+\Delta W} \dot{D}(\xi_m,\eta_n,\omega)\boldsymbol{G}(\boldsymbol{x},\xi_m,\eta_n,\omega)e^{-i\omega(\tau_{mn}+t_{mn})}d\xi d\eta \tag{8}$$

In order to take into account the difference between the slip time function of the large fault and that of the small fault, the transfer function is introduced, which is defined as:

$$T_{mn}(\omega) = \frac{\dot{D}(\xi_m,\eta_n,\omega)}{\dot{D}_{mn}(\xi_m,\eta_n,\omega)} \tag{9}$$

where $\dot{D}_{mn}(\xi_m,\eta_n,\omega)$ is the Fourier transform of the velocity of the slip time function at position (ξ_m,η_n) of the small fault. Using Eq.(9), Eq.(8) can be written as:

$$\boldsymbol{u}(\boldsymbol{x},\omega) = \sum_{m=1}^{N_L}\sum_{n=1}^{N_W} T_{mn}(\omega)\boldsymbol{u}_{mn}(\boldsymbol{x},\omega) \tag{10a}$$

where

$$\boldsymbol{u}_{mn}(\boldsymbol{x},\omega) = \int_{\xi_m}^{\xi_m+\Delta L}\int_{\eta_n}^{\eta_n+\Delta W} \dot{D}_{mn}(\xi_m,\eta_n,\omega)\boldsymbol{G}(\boldsymbol{x},\xi_m,\eta_n,\omega)e^{-i\omega(\tau_{mn}+t_{mn})}d\xi d\eta \tag{10b}$$

In Eq.(10b), $\boldsymbol{u}_{mn}(\boldsymbol{x},\omega)$ is the far-field displacement due to the small fault. Equation (10) indicates that the simulated motion of the large fault is the summation of contributions with weight $T_{mn}(\omega)$ from the $N_L \times N_W$ small faults.

Based on Eq.(10), an approximate simulation method can be obtained, using a single observation record $\boldsymbol{u}_0(\boldsymbol{x},\omega)$ due to the $(m_0,n_0)^{th}$ fault among small faults. By assuming that the slip time function of each small fault and the Green's function from the position of each small fault to the observation point are approximately equal to those of the $(m_0,n_0)^{th}$ fault, then Eq.(10a) can be reduced as:

$$\boldsymbol{u}(\boldsymbol{x},\omega) = \sum_{m=1}^{N_L}\sum_{n=1}^{N_W}\frac{R_0}{R_{mn}}T_{mn}(\omega)e^{-i\omega(\tau_{mn}+t_{mn})}\boldsymbol{u}_0(\boldsymbol{x},\omega) \tag{11}$$

In deriving Eq.(11) the effect of the hypocentral distance on the Green's function has been considered approximately because the shear wave attenuates inversely proportional to the hypocentral distance in a homogeneous isotropic medium. From the similarity conditions of earthquakes (Kanamori *et al.*, 1975), the following relations are derived:

$$(\frac{M_0}{m_0})^{1/3} = \frac{L}{\Delta L} = \frac{W}{\Delta W} = \frac{D}{D_0} = \frac{\tau}{\tau_0} = N_L = N_W = N \tag{12}$$

where M_0 is the seismic moment of the large fault: m_0 the seismic moment of the small fault; D and τ are the final offset of the dislocation and the dislocation rise time of the large fault, respectively; D_0 and τ_0 those of the small fault.

The transfer function $T_{mn}(\omega)$ defined by Eq.(9) can be obtained by specifying a slip time function. The following transfer function is used in this paper:

$$T_{mn}(\omega) = \left[\frac{i\omega + \frac{N}{\tau}}{i\omega + \frac{1}{\tau}}\right]\left[\frac{1+\kappa(\frac{\omega\tau}{2})^2}{1+(\frac{\omega\tau}{2})^2}\right] \tag{13}$$

where κ is a parameter that controls the value of the transfer function in high frequency range. Although several physical models exist (Aki and Richards, 1980), the generation process of high frequency seismic waves due to fault rupture may be quite complex. Therefore, without the use of physical models, one parameter κ has been introduced here, which has to be empirically estimated. For $\kappa = 1$, the transfer function is equivalent to that obtained by assuming the exponential function for slip time function of the large fault and the small fault (Harada *et al.*, 1995). It is noted here that the several transfer functions examined in this paper (see numerical examples) are obtained by assuming the ramp function for slip time function (Harada *et al.*, 1995) and the Irikura model (1983). It is also noted here that the frequency variations of the different transfer functions examined in this paper are similar in the low frequency range; and, in the high frequency range, the transfer function obtained from the assumption of the ramp function for slip time function takes value lower than the other transfer functions.

Average Characteristics of the Source Spectrum of an Extended Fault

To show the average characteristics of the source spectrum of an extended fault, we assume that the rupture start times of each small fault are distributed randomly with uniform probability over the rupture duration T of an extended fault. By considering the practical situation, the small faults are assumed identical so that a single observation record from a specific small fault can be used. For the attention of the source characteristics, we neglect the correction of the hypocentral distances. With these assumptions the Fourier spectrum of the uni- component waveform $u_S(\omega)$ from an extended fault may be written such as:

$$u_S(\omega) = \sum_{m=1}^{N}\sum_{n=1}^{N} T_{mn}(\omega) e^{-i\omega t^*_{mn}} u_{S0}(\omega) \tag{14}$$

where $u_{S0}(\omega)$ represents the Fourier spectrum of the uni-component waveform from the small fault, and t^*_{mn} the time delay uniformly distributed over the rupture duration T. By taking the expectation over the ensemble, the average source spectrum $|u_S(\omega)|$ is obtained as:

$$|u_S(\omega)| = SUM_N(\omega)|T(\omega)||u_{S0}(\omega)| \tag{15}$$

where $|T(\omega)|=|T_{mn}(\omega)|$ is the transfer function given by Eq.(13), and $SUM_N(\omega)$ the coefficient of random summation given such as:

$$SUM_N(\omega) = \sqrt{N^2\left[1+(N^2-1)\left(\frac{\sin(\frac{\omega}{\omega_f})}{(\frac{\omega}{\omega_f})}\right)^2\right]} \tag{16}$$

In Eq.(16), ω_f is the first corner frequency determined from the rupture duration of an extended fault such as:

$$\omega_f = \frac{2}{T} \tag{17}$$

By introducing the second and third corner frequencies defined by,

$$\omega_c = \frac{2}{\tau}, \qquad \omega_{c0} = \frac{2}{\tau_0} \tag{18}$$

the transfer function of Eq.(13) can be rewritten as:

$$T(\omega) = T_{mn}(\omega) = \left[\frac{N + i(2\frac{\omega}{\omega_c})}{1 + i(2\frac{\omega}{\omega_c})}\right]\left[\frac{1 + \kappa(\frac{\omega}{\omega_c})^2}{1 + (\frac{\omega}{\omega_c})^2}\right] \tag{19}$$

where,

$$N = (\frac{M_0}{m_0})^{1/3} = \frac{\omega_{c0}}{\omega_c} \tag{20}$$

The source spectrum of the small fault is assumed to be ω^{-2} model such as:

$$|u_0(\omega)| = \frac{m_0}{1 + (\frac{\omega}{N\omega_c})^2} \tag{21}$$

In the two extreme frequencies where $\omega \to 0$ and $\omega \to \infty$, the source spectrum of an extended fault is found from Eq.(15) to be given by:

$$|u_S(\omega)| = \begin{cases} N^3 m_0 = M_0 & \omega \to 0 \\ \kappa M_0 \left(\frac{\omega_c}{\omega}\right)^2 & \omega \to \infty \end{cases} \tag{22}$$

Figures 2 and 3 show the source spectra of extended fault normalized by the seismic moment M_0 for the cases of κ=1 and 5, respectively. In each figure, ω_f/ω_c =1/10 is assumed and the variations with the summation parameter N are shown. For comparison, the ω^{-2} source model with the second corner frequency ω_c is shown by the heavy line in each figure. It is found from Fig.2 (for the case of κ =1) that the source spectrum of extended fault follows the ω^{-2} model at the lower frequency (ω_f) and the higher frequency (ω_{c0}) limits, but at intermediate frequency range its spectral amplitude is lower as the summation parameter N increases than that expected from the ω^{-2} model. These characteristics observed from Fig.2 are also observed from Fig.3 (for the case of κ=5), but the source spectral amplitude is amplified by a factor of κ at higher frequency range ($\omega \geq \omega_{c0}$).

By comparing these characteristics shown in Figs. 2 and 3 with those obtained from the various irregular source models (for examples, Sato *et al.*, 1973, Hanks *et al.*, 1981, Papageorgious *et al.*, 1983, Izutani, 1984) where the heterogeneity of either slip or stress drop on the extended fault plane is taken into account, the parameter κ may be found to be equivalent to the ratio of local stress drop to global stress drop or the ratio of dynamic stress drop to static stress drop.

NUMERICAL EXAMPLES

Numerical examples (Harada, *et al.*, 1995a) are given now in order to demonstrate an applicability of the simulation method using a stochastic point source model and the simulation method of strong motion derived from an extended fault into an artificial generation of strong motions for aseismic design. The examples are also given to visualize the effect of the transfer functions on the simulated ground acceleration motions.

The geometrical relations of the large earthquake (extended fault), the small earthquake, and the observation point used in the numerical examples are shown in Fig.4 . The source parameters of the large earthquake and the small earthquake are indicated in Tables 1 and 2. Figure 5 shows a sample acceleration motion of the small earthquake with magnitude 5, R_0=20 km, and Δ=17.32 km generated using Eq.(1) with time interval Δt = 0.01 sec, and $\omega_u = 2\pi \times 50$ rad/sec, N_ω=1024. In this simulation, the following values are used:

$$R(\theta, \varphi) = 0.63; \quad F = 2.0; \quad V = 0.5; \quad \rho = 2.7\text{gr/cm}^3; \quad C_S = 3.6\text{km/sec}; \quad \omega_c = 7.07\text{rad/sec} \tag{23a}$$

$$\omega_{max} = 66.4\text{rad/sec};\ Q = 10^{(q_1 \log(\omega/2\pi) + q_2)};\ q_1 = 0.64;\ q_2 = 2.1;\ \omega_g = 5.56\text{rad/sec};\ h_g = 0.6 \quad (23b)$$

Figure 6 shows the acceleration motions from the large earthquake simulated by Eq.(11) using the simulated motion of the small earthquake in Fig.5. In this simulation $N = 8$ is decided from Eq.(12) and Tables 1 and 2. It is seen from Fig.6 that the acceleration motions simulated by the method using transfer functions of the Brune model (by assuming the exponential function for slip time function), the Irikura model (Irikura, 1988), and the proposed model ($\kappa = 1$) are similar, while the motion simulated by the method using transfer function of the Haskell model (by assuming the ramp function for slip time function) has lower amplitude. In the proposed model, the peak acceleration is found to be controlled by the parameter κ.

CONCLUSIONS

This paper describes digital simulation methods of strong earthquake ground motions using a seismological model. It can be concluded that:

1) A simulation method of ground motion using a stochastic point source model has been described.
2) The Kanai-Tajimi spectrum is improved by taking into account the seismological source model.
3) A simulation method of strong ground motion from an extended fault has been described. The method is based on the representation theorem of elastodynamics in the frequency domain. In this method, the simulated motion derived from a stochastic point source model is used as the small earthquake ground motion rather than the recorded motion as is usually done in the empirical Green's function method
4) A new transfer function which takes into account the difference between the slip time function of the large earthquake and that of the small earthquake is presented.
5) The new parameter κ introduced into the new transfer function is found to be equivalent to the ratio of local stress drop to global stress drop or the ratio of dynamic stress drop to static stress drop in the available irregular source models where the heterogeneity of either slip or stress drop on the extended fault plane is taken into account.

In the paper (Harada *et al.*, 1995b), the proposed simulation methods are examined by comparing with the observed records at Miyazaki city during the Hyuganada earthquake (M_{JMA}=6.6, 3/18, 1987) and its aftershock (M_{JMA}=5.0). From this examination, it is found that the proposed method can predict the observed records if we could predict the appropriate parameters in the model. In this specific earthquake case, the parameter κ is found to be 1.3-3.0.

REFERENCES

1) Aki, K., and Richards, P.G. (1980), *Quantitative Seismology, Vol.I and Vol. II*, W.H. Freeman and Company.
2) Clough, R.W., and Penzien, J. (1975), *Dynamics of Structure*, McGraw-Hill, pp.614.
3) Hanks, T.C., and McGuire, R.K. (1981), The Character of High-Frequency Strong Ground Motion, *Bull. of Seism. Soc. of Am., Vol.71*, pp.2071-2095.
4) Hartzell, S.H. (1978), Earthquake Aftershock as Green's Functions, *Geophys. Res. Lett., Vol.5*, pp.5.
5) Harada, T., and Tanaka, T. (1995a), Digital Simulation of Earthquake Ground Motions using a Seismological Model, *Journal of Structural Mechanics and Earthquake Engineering, JSCE, No.507/I-30*, pp.209-217.
6) Harada, T., and Tanaka, T. (1995b), Digital Simulation of Ground Motions using Stochastic Green's Function and Its Verification, *Proc. of the 3rd Japan Conference on Structural Safety and Reliability*, Nobember, Tokyo, pp.527-534.
7) Irikura, K. (1983), Semi-Empirical Estimation of Strong Ground Motions during Large Earthquakes, *Bull. of Disaster Prevention Research Institute, Kyoto University, Vol.32*, pp.63-104.
8) Irikura, K. (1988), Prediction of Strong Accelerations Motions using Empirical Green's Function, *Proc. of 7th Japan Earthquake Engineering Symposium*, pp.37-42.
9) Izutani, Y. (1984), Source Parameters Relevant to Heterogeneity of a Fault Plane, *J. Phys. Earth, Vol.32*, pp.511-529.
10) Kanai, K. (1957), A Semi-Empirical Formula for the Seismic Characteristics of the Ground Motions, *Bull. of Earthquake Research Institute, The University of Tokyo, Vol.35*, pp.309-325.

11) Kanamori, H., and Anderson, D.L. (1975), Theoretical Basis of Some Empirical Relations in Seismology, *Bull. of Seism. Soc. of Am., Vol.65*, pp.1073-1095.
12) Kimura, K., and Kameda, H. (1987), Random Vibration Solution for Attenuation Equation of Earthquake Response Spectra Incorporating Nonlinear Soil Amplification, *Research Report No.87-2, School of Civil Engineering, Kyoto University.*
13) Papageorgiou, A.S. and Aki, K. (1983), A Specific Barrier Model for the Quantitative Description of Inhomogeneous Faulting and the Prediction of Strong Ground Motion I. Description of the Model, *Bull. of Seism. Soc. of Am., Vol.73*, pp.693-722.
14) Saikia C.K. (1993), Estimated Ground Motions in Los Angeles due to M=7 Earthquake on the ELysian Thrust Fault, *Bull. of Seism. Soc. of Am.. Vol.83*, pp.780-810.
15) Sato, T. and Hirasawa, T. (1973), Body Wave Spectra from Propagating Shear Cracks, *J. Phys. Earth, Vol.21*, pp.415-431.
16) Somerville, P., Sen, M. and Cohee, B. (1991). Simulation of Strong Ground Motions Recorded during the 1985 Michoacan, Mexico and Valparaiso, Chile Earthquakes, *Bull. of Seism. Soc. of Am., Vol.81*, pp.1-27.
17) Shinozuka, M., Deodatis, G., and Harada, T. (1987), Digital Simulation of Seismic Ground Motion, *Stochastic Approaches in Earthquake Engineering*, Edited by Lin, Y.K., and Minai, R., Springer-Verlag, pp.252-298.
18) Tajimi, H. (1960), A Statistical Method of Determining the Maximum Response of a Building Structure during a Earthquake, *Proc. of 2nd World Conference on Earthquake Engineering, Vol.2*, pp.781-797.

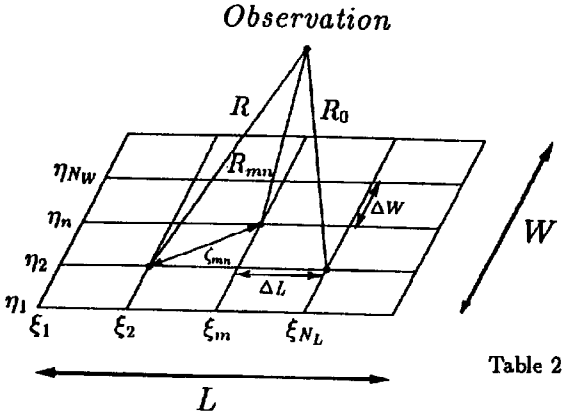

Figure 1 Schematic diagram of the Green's function method and its notations

Table 1 The source parameters of a large fault used in the numerical examples

Parameters Name	*Value*	*Unit*
Strike	$N60.6°E$	
Slip Type	Strike Slip	
Dip Angle	90	degree
Length	20	km
Width	10	km
Depth of top of fault	0	km
Seismic Moment	2.04×10^{26}	dyne-cm
Magnitude	7	
Rise Time	1.6	sec
Rupture Velocity	2.5	km/sec
S Wave Velocity	3.6	km/sec

Table 2 The source parameters of a small fault used in the numerical examples

Parameters Name	*Value*	*Unit*
Seismic Moment	4.47×10^{23}	dyne-cm
Magnitude	5	
Hypocentral Distance	20	km

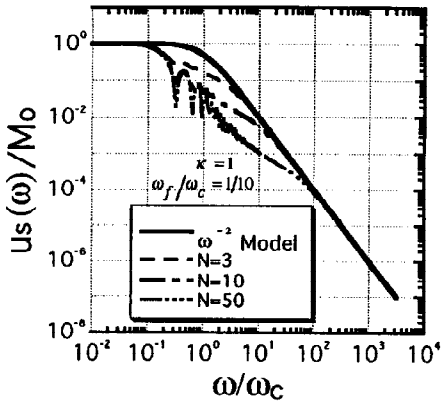

Figure 2 Normalized spectra of the large earthquake by a ramdom summation of the small earthquakes,compared to the ω^{-2} spectrum (heavy line). (In the case of $\kappa = 1$)

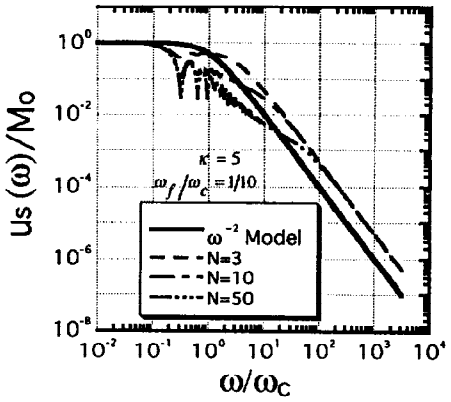

Figure 3 Normalized spectra of the large earthquake by a ramdom summation of the small earthquakes,compared to the ω^{-2} spectrum (heavy line). (In the case of $\kappa = 5$)

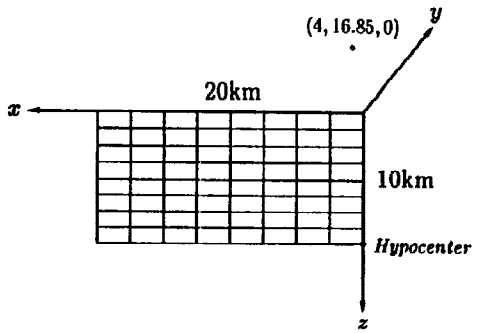

Figure 4 A large fault, a small fault, and the observation point used in the numerical examples

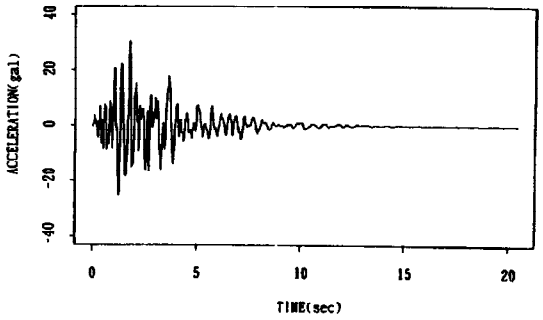

Figure 5 A simulated sample ground acceleration from a small earthquake

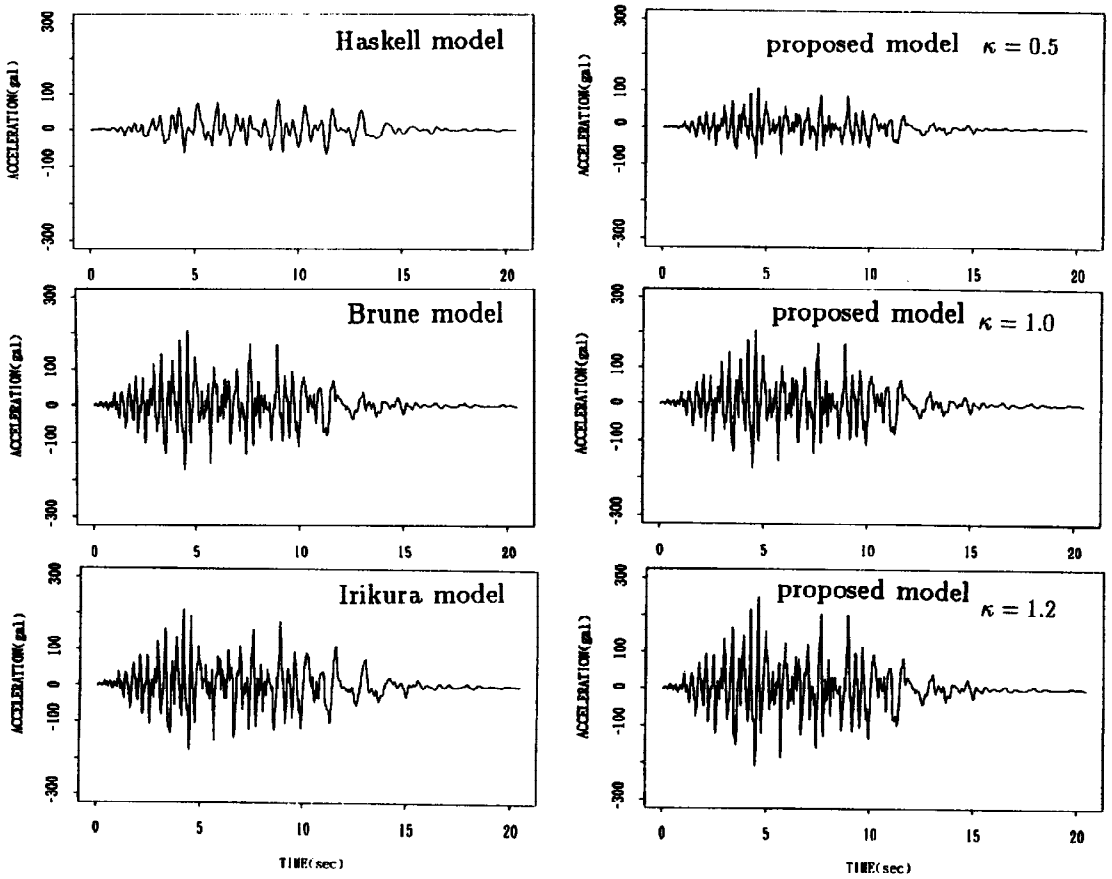

Figure 6 A simulated sample ground accelerations from a large earthquake for the different models